

AgileFormer: Spatially Agile Transformer UNet for Medical Image Segmentation

Peijie Qiu, Jin Yang, Sayantan Kumar, Soumyendu Sekhar Ghosh, Aristeidis Sotiras
Washington University in St. Louis, St. Louis, MO, USA
<https://github.com/sotiraslab/AgileFormer>

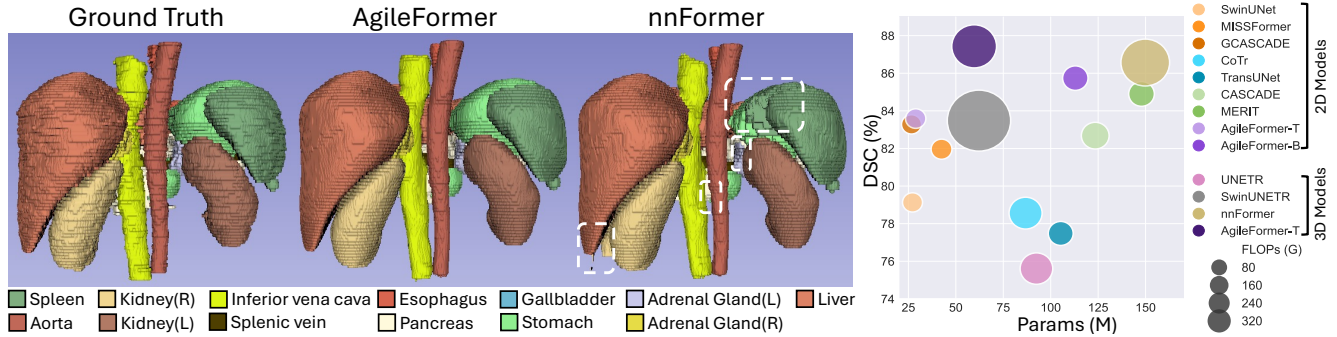


Figure 1. **Left:** Qualitative comparison between the proposed AgileFormer and nnFormer [47] on the Synapse multi-organ segmentation task, where each white dashed box marks inaccurate segmented regions. For demonstration purposes, we visualize all 13 organs, but we only report results for 8 of them. We can observe that nnFormer struggled to accurately segment the spleen and stomach, confusing one for the other. Moreover, it over-segmented the right kidney. This is likely due to the fact that fixed-sizing window attention and patch embedding cannot accurately capture objects with varying sizes and shapes, and hence produce inaccurate feature representations. In contrast, AgileFormer, which can capture spatially varying representations via deformable patch embedding, spatially dynamic self-attention and multi-scale deformable positional encoding, accurately segmented organs with varying sizes and shapes. **Right:** Segmentation accuracy (DSC) against model complexity (number of parameters and FLOPs) on the Synapse multi-organ segmentation task. In both 2D and 3D settings, AgileFormer outperformed recent state-of-the-art methods, while having fewer parameters and FLOPs.

Abstract

In the past decades, deep neural networks, particularly convolutional neural networks, have achieved state-of-the-art performance in a variety of medical image segmentation tasks. Recently, the introduction of vision transformers (ViTs) has significantly altered the landscape of deep segmentation models. The excellent performance and scalability of ViTs have driven a growing focus on their application. However, we argue that the current design of the vision transformer-based UNet (ViT-UNet) segmentation models may not effectively handle the heterogeneous appearance (e.g., varying shapes and sizes) of target objects. In addition, prevailing ViT-UNets focus on enhancing the self-attention building block while neglecting other important components (i.e., patching embedding and positional encoding). To tackle these limitations, we present a structured approach to introduce spatially dynamic components into a ViT-UNet. This enables the model to effectively capture

features of target objects with diverse appearances. This is achieved by three main components: (i) deformable patch embedding; (ii) spatially dynamic multi-head attention; (iii) multi-scale deformable positional encoding. These components are integrated into a novel architecture, termed **AgileFormer**. Experiments in three segmentation tasks using publicly available datasets (Synapse multi-organ, ACDC cardiac, and Decathlon brain tumor datasets) demonstrated the effectiveness of AgileFormer for 2D and 3D segmentation tasks. Remarkably, AgileFormer sets a new state-of-the-art performance with a Dice Score of **85.74%** and **87.43%** for 2D and 3D multi-organ segmentation on Synapse without significant computational overhead.

1. Introduction

Medical image segmentation tasks are important in modern medicine, as they typically serve as the first step in many image-driven diagnoses and analyses [4, 5]. Deep learn-

ing based automated segmentation methods have dominated this field due to their high efficiency and state-of-the-art performance. Among them, convolutional neural networks (CNNs) [17, 18, 20, 26, 30] have emerged as the prevalent choice since the introduction of UNet [30]. This is due to CNNs’ inherent advantages in handling image-driven tasks, such as their ability to capture locality and translation invariance. However, they struggle with capturing global semantics primarily due to their restricted receptive field.

In contrast, the recently proposed vision transformer (ViT) [8] mitigates this problem through a self-attention mechanism that captures dependencies between image patches regardless of their spatial distances. The first ViT-based UNet (ViT-UNet) for medical image segmentation combined a ViT encoder with a CNN decoder, and hence was termed TransUNet [5]. However, TransUNet is burdened by a large number of parameters ($\sim 100M$) and considerable computational complexity. This is because it employs standard self-attention, which has quadratic time and memory complexity w.r.t. the input token size. SwinUNet [23] addressed this challenge by leveraging window attention [23], which performs self-attention within small windows in parallel for all image patches. SwinUNet is the first pure ViT-UNet, with self-attention as the main feature extractor for the encoder, decoder, and bottleneck of a UNet. However, SwinUNet uses fixed-size windowing, which may limit its ability to capture precise representations for target objects with varying sizes and shapes. Additionally, previous ViT-UNets deploy a fixed-size patch partitioning (i.e., patch embedding), which inherently limits their ability to localize objects with varying sizes and shapes (see evidence in Fig. 1 (Left) and Fig. 6 (a)). Because objects are not always perfectly bounded by fixed-size square patches.

We argue that the inability of standard ViT-UNets to capture spatially heterogeneous representations restricts their scalability and adaptability to various segmentation tasks, especially those involving heterogeneous targets. One notable example is the multi-organ segmentation task, where TransUNet and SwinUNet do not exhibit good scalability when increasing the number of parameters (as evident in Fig. 5). In contrast, models that can capture spatially varying representations (i.e., CoTr [41] and MERIT [29]) showed better scalability. However, the building block in the encoder and decoder of CoTr remains convolutional layers with the bottleneck replaced by a Deformable DETER [49]. MERIT [29] only captures multi-scale feature representations by having a multi-resolution input, which may fail to capture feature representation with varying shapes. We kindly direct readers to Appendix A for a more detailed comparison of the proposed method with CoTr and MERIT. Furthermore, the adaptability of ViT-UNet deteriorates when training samples are extremely scarce. This is particularly true in 3D

multi-organ segmentation with only 18 training samples, where SwinUNETR [10] and nnFormer [47] did not empirically show superior performance compared to CNN-based nnUNet [17]. We conjecture that the hierarchical feature extraction in CNNs naturally captures structures within objects at multiple scales. However, this is more challenging for fixed-size window attention and patch embedding in SwinUNet and nnFormer.

Contributions: To address limitations in previous ViT-UNet designs, we propose a spatially agile pure ViT-UNet to capture diverse target objects in a medical image segmentation task. We introduce a structured approach to introduce spatially dynamic components that can capture objects with varying sizes and shapes into a standard ViT-UNet. First, we replaced the standard rigid square patch embedding in ViT-UNet with a novel deformable patch embedding. Second, we adopted spatially dynamic self-attention [40] as the building block to capture spatially varying features. Third, we proposed a novel multi-scale deformable positional encoding to model irregularly sampled grids in self-attention. We integrated these dynamic components into a novel ViT-UNet architecture, named **AgileFormer**.

We validated our method on three medical image segmentation tasks, including multi-organ, cardiac, and brain tumor MRI segmentation. Extensive experiments demonstrated the effectiveness of the proposed method for three medical image segmentation tasks. Specifically, AgileFormer outperformed recent state-of-the-art UNet models for both 2D and 3D medical image segmentation across all three segmentation tasks, demonstrating exceptional scalability. Remarkably, AgileFormer set a new state-of-the-art performance for multi-organ segmentation, achieving an average DSC (%) of 85.74 and 87.43 in 2D and 3D settings with fewer parameters and FLOPs (see Fig. 1 (Right)). Importantly, our empirical investigations also revealed critical components (i.e., patch embedding and positional encoding) in designing a ViT-UNet, which was neglected by previous works but has a significant impact on performance.

2. Related work

CNN-based segmentation methods: During the past decade, convolutional neural networks (CNNs) have been considered the defacto standard for medical image segmentation following the emergence of UNet [30]. Many follow-up works extend the U-shaped encoder-decoder network by introducing different skip-connection methods, including attention-based skip-connection (e.g., Attn-UNet [26] and UCTransUNet [36]) and dense skip-connection (e.g., UNet++ [48] and UNet 3+ [13]). Another line of works modified the convolution building block in UNet by introducing residual connection [18, 45], deformable convolution [22], and large kernel convolution [20, 21, 43]. In addition, methods that leverage multi-scale information for

capturing representation at varying sizes have been investigated [31, 46]. Previous work also explored a generalized UNet framework, termed nnUNet [17], which provides a self-configuring UNet framework for any dataset. Finally, MedNeXt [32] extended nnUNet by proposing a transformer-like architecture design of nnUNet following the advances in model designs outlined in ConvNeXt [24].

ViT-based segmentation methods: Since its introduction in 2020, ViT [8] has significantly shifted the trajectory of the design of UNets. This is because self-attention in ViTs is more advantageous in capturing long-range dependencies between image patches than convolution in CNNs. In particular, early explorations integrated ViTs into traditional CNN-based UNets by replacing the CNN encoder [5, 11] and bottleneck [38, 41] with a ViT. There are also hybrid models [12, 27, 28, 41], where the main feature extraction in the encoder/decoder is achieved by both CNN and ViT. However, due to the quadratic complexity and the lack of locality in standard self-attention, few pure ViT-based UNets [4, 16, 29, 47] have been proposed for medical image segmentation tasks, with most relying on the shifted window attention [23].

However, prevailing methods focus on advancing the self-attention building block in a ViT-UNet, while neglecting the other important components (e.g., patch embedding and positional encoding) in building a ViT-UNet. In contrast, our empirical findings revealed that the design of the patch embedding and positional encoding were equally important as the self-attention in enhancing the performance of a ViT-UNet. In addition, none of the prior ViT-UNets for medical image segmentation has explored capturing spatially dynamic feature representation to handle segmentation targets of varying sizes and shapes. In contrast, our Agileformer provides a systematical way to capture spatially dynamic feature representation by a novel deformable patch embedding, spatially dynamic self-attention, and deformable positional encoding.

3. Method

In this section, we provide a roadmap going from the standard SwinUNet to the proposed AgileFormer (see Fig. 2). To make this paper self-contained, we first provide a brief introduction of the essential elements in ViT-UNets. A ViT-UNet (e.g., SwinUNet) is a U-shaped encoder-decoder network with skip connections, wherein the primary feature extractions in both the encoder and decoder are achieved by the self-attention mechanism. The building block of a standard ViT-UNet is composed of three fundamental components: patch embedding, self-attention, and positional encoding. The patch embedding projects image patches into feature embeddings. More recent ViTs [39, 40] even treat downsampling (i.e., patch merging in a SwinUNet) as part of the patch embedding. In this paper, we

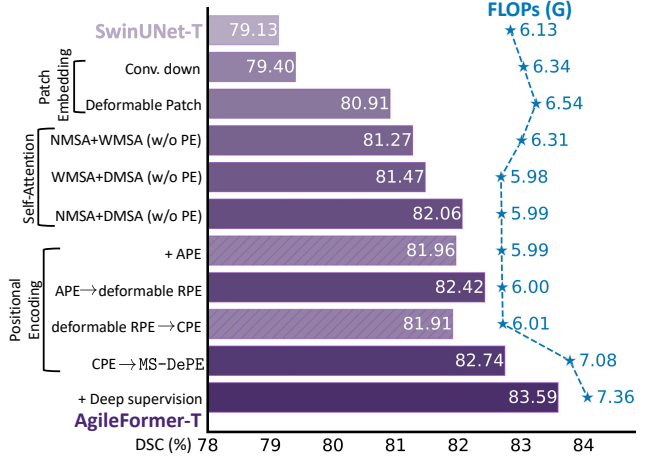


Figure 2. A roadmap going from a SwinUNet to the design of AgileFormer on Synapse dataset. From top to bottom, each row represents a model design variant, including patch embedding, self-attention, and positional encoding. The foreground bars represent DSC (%) in the FLOP (G) regime of different design variants; a hatched bar means the modification results in a performance drop.

will follow the same approach. The self-attention, which captures the dependencies between image patches, is used for the main feature extraction. For computational tractability and the need of locality, recent ViT-UNets use window-based self-attention mechanism [4, 10, 12, 15]. Unlike convolution, self-attention discards the spatial correlation between image patches, which hinders the localization ability of pure ViT in segmentation tasks. The positional encoding is used to address this limitation.

3.1. Deformable Patch Embedding

The ViT-UNet starts by converting image patches into tokens. This process typically involves partitioning an image into a sequence of non-overlapping $n \times n (\times n)$ square patches (e.g., 4×4 in SwinUNet [4] for 2D segmentation tasks and $4 \times 4 \times 4$ in nnFormer for 3D segmentation tasks). Subsequently, each of these patches is projected into a 1D feature vector. The main reason for performing a rigid (square) patch embedding is due to its simplicity, as it can be easily implemented as a standard convolution (kernel size $k = n$; stride $s = n$; dilation $d = 1$). However, we argue that this rigid patch embedding is not optimal for a segmentation task for two main reasons. First, segmentation requires more precise pixel-level localization. The rigid patch embedding can only provide patch-level localization. Second, the shape and size of target objects in most medical image segmentation tasks vary significantly.

Deformable patch embedding. To address the limitation of rigid patch embedding, we propose a deformable patch embedding (see Fig. 3) by leveraging the deformable con-

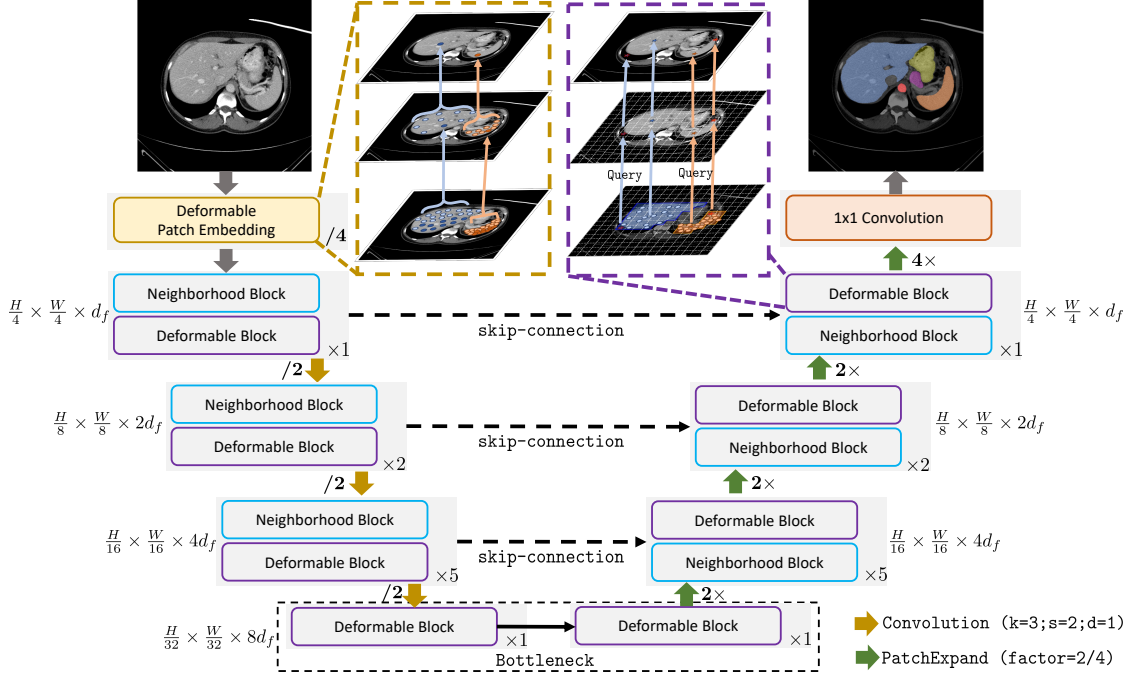


Figure 3. **The overview of the proposed AgileFormer.** AgileFormer is a U-shape vision transformer consisting of deformable patch embedding as well as neighborhood and deformable self-attention building block with a deformable positional encoding. For illustrative purposes, we take the 2D AgileFormer as an example. Please refer to Section 3.4 for the detailed discussion on extending 2D AgileFormer to 3D AgileFormer for volumetric segmentation tasks.

volution [7]. The deformable convolution is defined as

$$(\mathbf{f} * \mathbf{k})[p] = \sum_{p_k \in \Omega} \phi(\mathbf{f}; p + \Delta p + p_k) \cdot \mathbf{k}[p_k], \quad (1)$$

where $\mathbf{f} \in \mathbb{R}^{L \times d_f}$ is a d_f -dimensional feature map with a uniform grid of L locations $p \in \mathbb{R}^{L \times D}$ ($D = 2$ for 2D; $D = 3$ for 3D). \mathbf{k} is the convolutional kernel that operates on the grid $\Omega = [p_k]$ and defines the k -nearest (i.e., kernel size) neighboring locations of p . $[\Delta p]$ are offsets from which the irregular grid is sampled. The offsets are learned through a single convolutional layer $\Delta p = \text{Conv}_{\text{offset}}(\mathbf{f})$. ϕ is a sampling function that performs bilinear/trilinear interpolation to sample locations $[p + \Delta p + p_k]$ in \mathbf{f} , as the offsets Δp are typically fractional.

First patch embedding. We replaced the single-layer rigid convolution patch embedding in a standard SwinUNet with two consecutive deformable convolutional layers ($k = 3$; $s = n/2$; $d = 1$). The rationale behind this is that the two consecutive overlapping deformable patch embeddings can extract better local representations, which compensates for the lack of locality in the self-attention.

Downsampling patch embedding. We also replaced the patch merging in standard SwinUNet with convolutional downsampling via a single layer ($k = 3$; $s = 2$; $d = 1$). We used overlapping kernels to better preserve localized patterns [14, 39, 47], which also aligns with the overlapping

deformable patch embedding.

3.2. Spatially Dynamic Self-Attention

The self-attention is the building block of a ViT UNet. Unlike convolution, self-attention does not enforce any spatial inductive bias but makes decisions purely by relying on dependencies (mainly similarities) between tokens while lacking the ability to capture spatially adaptive features for multi-class segmentation. Accordingly, we propose using a spatially dynamic self-attention module as the building block of ViT-UNet. This module is inspired from [39], and it includes deformable multi-head attention (DMSA) [39] and neighborhood multi-head attention (NMSA) [9]. The transformer block was constructed by alternating these two attention mechanisms (see Fig. 3). We also distributed more computation to the third encoder block with a stage ratio of $[1 : 2 : 5 : 1]$, instead of $[2 : 2 : 2 : 2]$ as used in [4, 47]. This is because the third layer of the encoder typically captures better feature representations than other layers [36].

3.2.1 Deformable Multi-head Self-Attention

The deformable multi-head (i.e., H head) attention [39] for the h -th head is formulated as

$$\text{DMSA}_h(\mathbf{f}) = \text{softmax}(\mathbf{Q}_h \tilde{\mathbf{K}}_h^\top / \sqrt{d_k}) \tilde{\mathbf{V}}_h \quad (2)$$

where:

$$\begin{aligned} Q_h &= fW_h^Q, \quad \tilde{K}_h = \tilde{f}W_h^K, \quad \tilde{V}_h = \tilde{f}W_h^V \\ \text{with } \tilde{f} &= \phi(f; p + \Delta p_h). \end{aligned} \quad (3)$$

Here, we reuse the notation in Eq. (1) with p being a uniform grid of points, Δp_h being the generated offsets for the h -th head, and ϕ being an interpolation function. $\{W_h^Q, W_h^K\} \in \mathbb{R}^{d_f \times d_k}$ and $W_h^V \in \mathbb{R}^{d_f \times d_v}$ are trainable parameters, and d_k, d_v are the hidden dimensions of linear projection of the key \tilde{K}_h and the value \tilde{V}_h in DMSA. The offsets in DMSA are also generated by passing the query through a convolutional layer $\Delta p = \text{Conv}_{\text{offset}}(Q_h)$. The resulting irregularly sampled feature map is denoted as \tilde{f} in Eq. (3). Similar to deformable convolution, the irregularly sampled feature map is then applied to self-attention by using irregularly sampled key \tilde{K}_h and value \tilde{V}_h (see Eq. (2)).

3.2.2 Neighborhood Multi-head Self-Attention

In contrast to standard self-attention, which computes the similarity of each element at a given position p on a feature map f with every other element, the construction of neighborhood attention [9] only leverages the information from the k -nearest neighbors around location p . We reuse the notation k in Eq. (2), as the NMSA operates like a convolution. As a result, neighborhood attention reduces the quadratic computational complexity in standard self-attention to approximately linear w.r.t. the spatial dimension of f , as k is typically small (e.g., $k = 7 \times 7 (\times 7)$). Furthermore, this reintroduces local operations into self-attention, allowing for translational equivariance, and thereby enhancing the ability to better preserve local information. Following the notation in Eq. (2), the neighborhood multi-head attention at position p_l is computed as

$$\text{NMSA}_h(f[p_l]) = \text{softmax}(Q_h[p_l] \hat{K}_h[p_l]^\top / \sqrt{d_k}) \hat{V}_h[p_l]$$

where:

$$\begin{aligned} \hat{K}_h[p_l] &= [K_h[p_{l1}], \dots, K_h[p_{lk}]], \quad K_h = fW_h^K \\ \hat{V}_h[p_l] &= [V_h[p_{l1}]^\top, \dots, V_h[p_{lk}]^\top]^\top, \quad V_h = fW_h^V. \end{aligned}$$

Here, $[p_{lk}]$ denotes the k -th neighboring locations for a given location p_l . It is worth noting that the dimension of the resulting attention is $\mathbb{R}^{L \times K}$ with $K = k \times k (\times k)$, instead of $\mathbb{R}^{L \times L}$ in standard self-attention and window-attention.

3.3. Multi-scale Deformable Positional Encoding

The design of positional encoding (PE) is barely explored by previous ViT UNets. Most ViT-UNets either disregard positional encoding [5] or inherit PEs from their ancestor models [4, 12, 38]. Specifically, [38] used an absolute

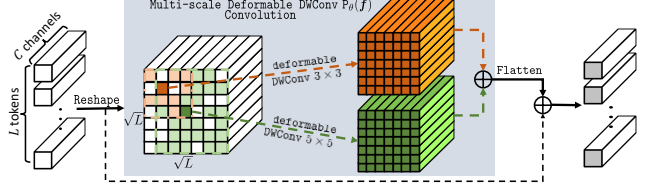


Figure 4. The proposed multi-scale deformable positional encoding (MS-DePE) for irregularly sampled grids in deformable multi-head self-attention. For illustrative purposes, we take the 2D model as an example, where 2D deformable depth-wise convolution is used. In the 3D model, the 2D deformable depth-wise convolution should be replaced with its 3D counterpart.

PE (APE), which assigns an absolute value for each token. While the others [4, 12, 47] used a relative PE (RPE) [34] to encode the relative positions between tokens. However, these are designed for 1D signals while neglecting spatial correlations. Consequently, they are not well adapted for modeling 2D/3D signals with spatial correlations. Recently, conditional PE (CPE) [6] was designed for vision tasks offering the ability of both APE and RPE at the same time. More importantly, standard APE, RPE, and CPE are not directly applicable to irregularly sampled grids, as all of them are formulated in a rigid grid. In accordance with the irregularly sampled DMSA presented in this paper, we propose a multi-scale deformable positional encoding (MS-DePE) designed to encode irregularly sampled positional grids across various scales (see Fig. 4).

The proposed MS-DePE is formulated in a conditional positional encoding fashion [6] as follows:

$$\text{MS-DePE}(f) = f + P_\theta(f),$$

where f is the input feature map, and P_θ denotes the trainable positional encoding layer parameterized by θ . P_θ is implemented as multi-scale deformable depth-wise convolutional layers with different kernel sizes (i.e., $3 \times 3 (\times 3)$ and $5 \times 5 (\times 5)$). For this purpose, we first recover the spatial resolution of the feature map f before passing it through P_θ . After applying P_θ , we reshape the feature map back to its original shape (see Fig. 4 for details).

3.4. Model Configurations

2D AgileFormer. Similar to [4, 5, 29], we developed two variants of AgileFormer by varying the embedding dimension (d_f) and the number of heads (H), while keeping the main structures unchanged (i.e., number of transformer blocks in the encoder/decoder): AgileFormer-T(iny) ($d_f = [64, 128, 256, 512]$; $H = [2, 4, 8, 16]$) and AgileFormer-B(ase) ($d_f = [128, 256, 512, 1024]$; $H = [4, 8, 16, 32]$). We also incorporated deep supervision (DS) outlined in [18, 47] into the proposed method.

Table 1. Performance comparison with 2D and 3D segmentation networks in the multi-organ segmentation using the Synapse multi-organ segmentation dataset. The best result for 2D and 3D models within each column is highlighted by **bold**, and the second-best is highlighted with an underline. [†]: models implemented by us. The other benchmarks were taken from [4, 5, 12, 16, 27, 29, 37, 42, 47].

Methods	Avg. DSC↑	HD95↓	Aorta	Gallbladder	Kidney(L)	Kidney(R)	Liver	Pancreas	Spleen	Stomach	
2D Models	U-Net [30]	76.85	39.70	89.07	69.72	77.77	68.60	93.43	53.98	86.67	75.58
	Att-UNet [26]	77.77	36.02	89.55	68.88	77.98	71.11	93.57	58.04	87.30	75.75
	TransUNet [5]	77.48	31.69	87.23	63.13	81.87	77.02	94.08	55.86	85.08	75.62
	MixedUNet [37]	78.59	26.59	87.92	64.99	81.47	77.29	93.06	59.46	87.75	76.81
	†CoTr [41]	78.56	24.05	87.09	65.37	86.19	80.32	94.22	52.28	87.01	76.00
	Hiformer [12]	80.69	19.14	87.03	68.61	84.23	78.37	94.07	60.77	90.44	82.03
	PVT-GCASCADe [28]	83.28	15.83	88.05	74.81	88.02	84.83	95.38	69.73	91.92	83.63
	▽Trans-CASCADE [27]	82.68	17.34	86.63	68.48	87.66	84.56	94.43	65.33	90.79	83.69
	R50 ViT [5]	71.29	32.87	73.73	55.13	75.80	72.20	91.51	45.99	81.99	73.95
	SwinUNet [4]	79.13	21.55	85.47	66.53	83.28	79.61	94.29	56.58	90.66	76.60
	TransDeepLab [2]	80.16	21.25	86.04	69.16	84.08	79.88	93.53	61.19	89.00	78.40
	†SDAUT [15]	80.67	25.59	87.03	69.30	81.87	80.20	94.91	64.56	89.54	77.91
	CATFormer [44]	82.17	16.20	88.98	67.16	85.72	81.69	95.34	66.53	90.74	81.20
	MissFormer [16]	81.96	18.20	86.99	68.65	85.21	82.00	94.41	65.67	91.92	80.81
	▽MERIT [29]	84.90	13.22	87.71	74.40	87.79	84.85	95.26	71.81	92.01	85.38
	AgileFormer-T w/o DS	82.74	19.28	88.08	75.16	82.41	81.36	95.09	67.23	90.94	81.61
	AgileFormer-T w/ DS	83.59	15.09	88.81	74.43	84.61	82.78	95.48	69.45	90.14	83.05
AgileFormer-B w/o DS	84.14	15.27	87.76	74.71	86.69	83.81	95.31	68.28	91.00	85.58	
AgileFormer-B w/ DS	85.74*	18.70	89.11	77.89	88.83	85.00	95.64	71.62	92.20	85.63	
3D Models	nnUNet [17]	86.99	10.78	93.01	71.77	85.57	88.18	97.23	83.01	91.86	85.26
	UNETR [11]	79.56	22.97	89.99	60.56	85.66	84.80	94.46	59.25	87.81	73.99
	SwinUNETR [10]	83.48	10.55	91.12	66.54	86.99	86.26	95.72	68.80	95.37	77.01
	nnFormer [47]	86.57	10.63	92.04	70.17	86.57	86.25	96.84	83.35	90.51	86.83
	AgileFormer-T w/ DS	87.43*	7.81*	91.80	73.02	87.63	87.49	97.06	82.05	95.88	84.48

*: $p < 0.05$; with Wilcoxon signed rank test to the second-best model. [∇]: Large models that have similar parameters to the AgileFormer-B model (Fig. 1 (Right)), where deep supervision is also applied. **Note**: All 2D AgileFormer results reported in this paper use the checkpoint from the last training epoch. If using the testing set to select the best model (e.g., as done in the code of MERIT, Trans-CASCADE, and PVT-GCASCADe), 2D Agileformer-B can achieve a DSC (%) and HD95 of 86.11 and 12.88.

3D AgileFormer. For 3D models, we only evaluated the tiny model (i.e., AgileFormer-T) that has a comparable size to other baseline models. We also used the same d_f and H as in the 2D model. However, we made a few modifications to accommodate the 3D input. First, we replaced 2D convolutions with 3D convolutions to generate the offset points ($\text{Conv}_{\text{offset}}(Q_h)$). Second, we sampled positions in the 3D grid based on the generated offset points. Third, for the key and query projection in DMSA, we kept 2D 1×1 convolutional projection. This is because 2D and 3D convolutions with a kernel size of 1 essentially perform the weighted summation over channels. Accordingly, we first reshaped the 5D tensor of size $[B \times C \times D \times H \times W]$ into a 4D tensor $[B \times C \times 1 \times (D * H * W)]$ and then performed a 2D 1×1 convolution. After finishing the computation of self-attention, we reshaped the 4D tensor back to 5D to restore its spatial dimension. Fourth, we replaced all 2D convolutions in the deformable patching embedding and multi-scale deformable positional encoding with 3D convolutions.

4. Experiments and Results

4.1. Experimental design

Dataset. In line with previous works [4, 5, 47], we validated the proposed method on three publicly available

medical image segmentation datasets: the Synapse multi-organ dataset [19], the Automated Cardiac Diagnosis Challenge (ACDC) dataset [3], and the brain tumor segmentation dataset from the Decathlon challenge [1]. The Synapse multi-organ dataset includes 30 3D abdominal CT scans with corresponding segmentation masks of 13 organs. For brevity, we refer to this dataset as Synapse hereafter. As consistent with prior works, we report the performance on 8 abdominal organs (i.e., aorta, gallbladder, kidney left, kidney right, liver, pancreas, spleen, stomach). The ACDC dataset consists of 100 3D cardiac MRI scans, each with a segmentation mask that features the right ventricle (RV), myocardium (Myo), and left ventricle (LV). The Decathlon brain tumor dataset comprises 484 3D multi-modal brain tumor MRI scans with segmentation masks delineating enhancing tumor, non-enhancing tumor, and edema. To be consistent with previous works [11, 47], we reported the results of the whole tumor (WT), enhancing tumor (ET) and tumor core (TC).

Experimental setup and evaluation metric. We evaluated the performance of both 2D AgileFormer (trained using slices) and 3D AgileFormer (trained using volumes), as previous works involved both 2D and 3D models. For 2D AgileFormer, we adhered to the experimental protocols outlined in [4, 5] for the Synapse and ACDC datasets, in-

Table 2. Performance comparison with 2D and 3D segmentation models in cardiac MRI segmentation using the ACDC dataset. †: models implemented by us. The other benchmarks were taken from [4, 5, 16, 27, 29, 37, 47].

Methods		Avg. DSC↑	RV	Myo	LV
2D Models	TransUNet [5]	89.71	88.86	84.53	95.73
	†CoTr [41]	90.52	87.81	88.44	95.29
	SwinUNet [4]	90.00	88.55	85.62	95.83
	MixedUNet [37]	90.43	86.64	89.04	95.62
	MissFormer [16]	90.86	89.55	88.04	94.99
	†SDAUT [15]	91.08	89.37	88.58	95.28
	▽PVT-CASCADDE [27]	91.46	88.00	89.97	95.50
	▽Trans-CASCADE [27]	91.63	89.14	90.25	95.50
	†MERIT [29]	91.81	90.44	89.12	95.85
	AgileFormer-T w/ DS	91.76	89.80	89.71	95.77
AgileFormer-B w/ DS	92.55*	91.05	90.40	96.19	
3D Models	UNETR [11]	88.61	85.29	86.52	94.02
	UNETR++ [33]	92.83	91.89	90.61	96.00
	PHTrans	91.79	90.13	89.48	95.76
	nnUNet [17]	91.61	90.24	89.28	95.36
	†nnFormer [47]	91.84	90.91	89.44	95.17
	AgileFormer-T w/ DS	92.07*	90.59	89.80	95.81

*: $p < 0.05$; with the paired t-test to the second-best model. We reproduce the results of nnFormer by taking the model weights released by the authors in [47].

Table 3. Performance comparison with 3D segmentation models in brain tumor segmentation using the Decathlon dataset. †: models implemented by us.

Methods	Avg. DSC†	WT	ET	TC
†nnUNet [17]	85.2	91.0	80.3	84.1
†MedNext [32]	85.4	90.3	81.5	84.5
†TransUNet [5]	84.6	90.5	79.9	83.4
†TransBTS [38]	84.2	90.2	79.6	82.9
†CoTr [41]	84.1	91.2	78.7	83.2
†UNETR [11]	84.1	90.5	79.3	82.4
†UNETR++ [33]	85.2	91.0	80.1	84.2
†SwinUNETR [10]	84.9	90.7	80.5	83.5
†nnFormer [47]	84.9	91.4	79.2	84.0
AgileFormer-T w/ DS	85.7*	91.2	80.8	85.1

*: $p < 0.05$; with the paired t-test to the second-best model.

cluding training/testing partitioning, input image size (i.e., 224×224), data augmentations, model selection, and evaluations. For the 3D AgileFormer, we followed the experimental protocols specified in [47] for a fair comparison with the previous literature. The input image sizes for Synapse, ACDC, and Decathlon brain tumor datasets were set to $64 \times 128 \times 128$, $14 \times 160 \times 160$, and $96 \times 96 \times 96$ ¹, respectively. We evaluated the segmentation performance using the dice similarity coefficient (DSC) and 95% Haus-

¹We used an input size of $96 \times 96 \times 96$ instead of $128 \times 128 \times 128$ in nnFormer [47] for brain tumor segmentation. This is because most baseline methods [5, 10, 11, 38, 41] in nnFormer [47] were implemented in $96 \times 96 \times 96$, and hence show a huge performance difference.

dorff Distance (HD95). Statistical significance between the average DSC of the best and second-best model was estimated using the paired t-test. We emphasize that all competing methods applied on the Synapse, ACDC, and Decathlon datasets followed the same experimental protocols.

Implementation details. All 2D and 3D models were trained using a combination of DSC and cross-entropy loss [4, 47], employing an AdamW [25] optimizer with cosine learning rate decay. We initialized model parameters with ImageNet pre-trained weights. Since different hyperparameter settings were used for 2D and 3D experiments, we kindly direct readers to Appendix B for the detailed model and hyperparameter configurations for each task. All experiments were implemented using PyTorch and were performed on a Nvidia V100 GPU with 32GB memory.

4.2. Main results

Results of 2D Models. 2D AgileFormer performed better than the second-best 2D models (i.e., MERIT [29] for both tasks) by 0.84 and 0.23, in average DSC (%) on the Synapse and ACDC datasets, respectively. This improvement was shown to be statistically significant. Specifically, the proposed method achieved an average DSC (%) of 85.74, surpassing the other baseline methods in segmenting 6 out of 8 organs on the Synapse dataset (see Table 1; 2D Models). For the remaining two organs, the proposed method was ranked the second best. On the ACDC dataset, AgileFormer achieved an average DSC (%) of 92.55, surpassing all the baseline methods in segmenting RV, Myo, and LV (see Table 2; 2D Models). Qualitative results also supported the superiority of AgileFormer. While AgileFormer accurately segmented structures of interest, other methods either under- or over-segmented certain regions (see Fig. 6 (a) and (b)).

Results of 3D Models. When comparing 3D models, 3D AgileFormer also outperformed other state-of-the-art segmentation methods across all three segmentation tasks. Specifically, AgileFormer achieved an average DSC (%) of 87.43 and an average HD95 (mm) of 7.81, surpassing nnFormer by 0.86 and 2.82 in DSC and HD95, respectively (Table 1; 3D Models). On the ACDC dataset, AgileFormer achieved an average DSC (%) of 92.07, outperforming nnFormer by 0.23 (Table 2; 3D Models). On the brain tumor segmentation task, the proposed method achieved an average DSC (%) of 85.7, surpassing nnFormer by 0.8 (Table 3). In addition, AgileFormer showed high qualitative segmentation quality on 3D segmentation tasks (see Fig. 1 and Fig. 6 (c)). In summary, the proposed AgileFormer was more effective on multi-organ and brain tumor segmentation tasks, where target objects exhibit more heterogeneous appearances than those in cardiac segmentation.

Additional qualitative results on Synapse produced by 3D models are shown in Fig. S2, where AgileFormer show-

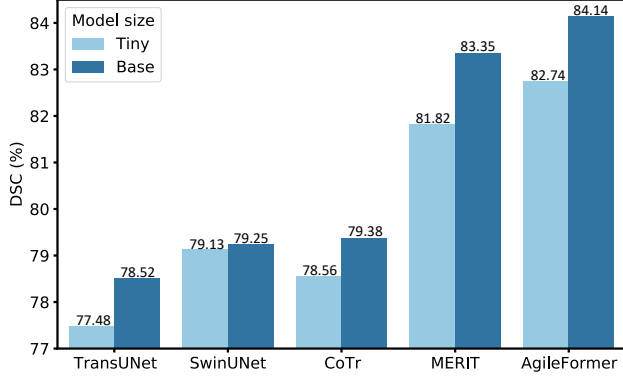


Figure 5. Comparison of model scalability on the Synapse dataset. The base model is almost four times larger than the tiny model. The proposed AgileFormer demonstrated exceptional scalability when adding parameters compared to other methods.

cased accurate segmentation compared to other state-of-the-art methods. Some failure cases on Synapse are shown in Fig. S3, where even methods that can extract spatially dynamic features (including AgileFormer) cannot accurately segment highly irregular organs such as Gallbladder and Pancreas. Similarly, Fig. S4 shows failure cases on brain tumor segmentation, where tissue classes with highly irregular appearance cannot be accurately segmented by most methods, including AgileFormer.

4.3. Ablations on model design variants

We conducted ablation studies on the model design variants on the Synapse dataset using 2D AgileFormer, including patch embedding and different choices of spatially dynamic attention and positional encoding (see Fig. 2). First, replacing patch merging with convolutional down-sampling led to a small performance gain of 0.34% in average DSC. Then, adding deformable embedding led to a performance gain of 1.9% in DSC. Second, we ablated different choices of spatially dynamic self-attention by alternating window/deformable/neighborhood attention. We removed positional encoding to eliminate its effect for now. Alternating window attention (WMSA) with both DMSA and NSMA led to a performance gain of 0.7% (DMSA) and 0.4% (NSMA), respectively. Alternating NSMA and DMSA resulted in a performance gain of 1.4%. Third, we brought back positional encoding, demonstrating that not all PEs can lead to a performance gain, e.g., adding APE and CPE even led to a performance drop. This is because these two PEs are not designed for irregularly sampled grids introduced by DMSA. Instead, the proposed MS-DePE improved performance by 0.8%. Notably, the proposed AgileFormer did not lead to a huge computational burden, with only a 1.1% increase in the number of parameters and a 15% rise in floating point operations, compared to SwinUNet.

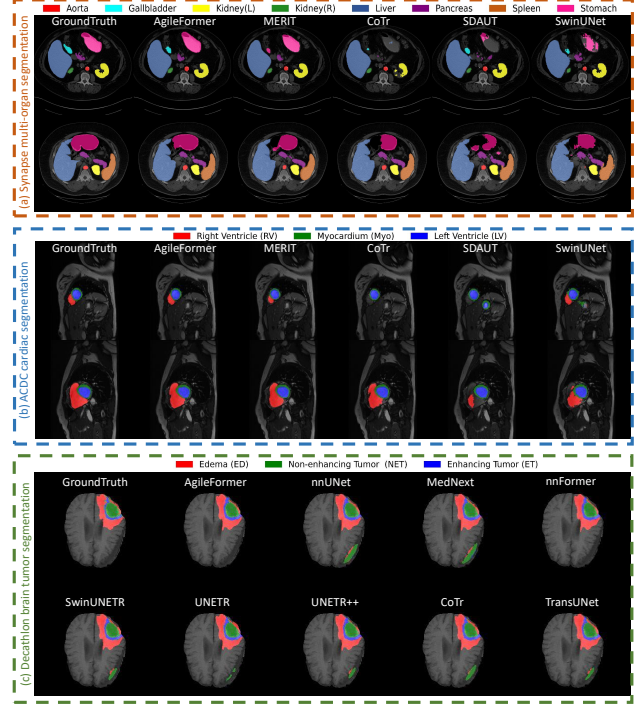


Figure 6. Visual comparison of (a) multi-organ, (b) cardiac, and (c) brain tumor segmentation across Synapse, ACDC, and DeCathlon datasets. AgileFormer showed the best qualitative segmentation quality across all three segmentation tasks.

4.4. Model scalability

We compared the scaling behavior of the proposed method with other ViT-UNets on the Synapse dataset using 2D AgileFormer. As shown in Fig. 5, the proposed method demonstrated improved performance with growing model sizes for the Synapse multi-organ segmentation task, where different organs exhibited a lot of variability in shape and size. Specifically, the performance was improved by 2.15 in DSC (%) going from AgileFormer-T to AgileFormer-B, with parameters increasing approximately fourfold from 28.85M to 123.47M. We also observed that the methods (i.e., CoTr, MERIT, and AgileFormer) can capture spatially varying representations generally scaled better than standard ViT-UNets (i.e., TransUNet and SwinUNet). However, CoTr did not scale as well as MERIT and AgileFormer. We hypothesized this might be attributed to the fact that the main backbone of CoTr was still a CNN. The deformable module in CoTr was only placed in the bottleneck.

4.5. Discussion

Failure cases: Although AgileFormer demonstrated improvements over previous state-of-the-art segmentation methods quantitatively and qualitatively, it still has limitations on highly irregular and unstructured objects (e.g.,

on Pancreas and Gallbladder (see Fig. S3) and some tissue classes in brain tumor segmentation (see Fig. S4)). This suggests that there is still room for improvement in future work with more powerful spatially varying components; whereas our investigation revealed the importance of incorporating spatially varying components into UNet designs.

Potential trade-offs between different organs: First, we observed that AgileFormer showed more promising results on challenging small and irregular organs (e.g., Gallbladder Aorta, and Pancreas) but also achieved the best performance on most large organs (see Table 1). Second, we observed that many ViT-UNets can perform equally well on the larger organs (e.g., Liver and Spleen). However, the pure CNN-based methods did not work well on the larger organs. We conjectured that this phenomena was attributed to the fact that the self-attention mechanism in ViT-UNets better capture global context than convolution in CNNs (which is typically limited by the receptive field). Third, CNN-based models (U-Net [30] and Att-UNet [26]) biased toward small organs (e.g., Aorta) due to the inherent locality of convolution in capture small objects. In contrast, the rigid patching embedding in ViT-UNets may fail to capture such localized structures and hence showed inferior performance on small organs. Notably, our investigation revealed that replacing the rigid patch embedding with a deformable patch embedding dramatically improved the performance of ViT-UNets on segmenting smaller organs (e.g., Aorta and Pancreas). Furthermore, our novel multi-scale deformable positional encoding improved the DSC (%) by 4.21% for Gallbladder segmentation.

5. Conclusion

In this paper, we proposed AgileFormer that introduced spatially dynamic components (i.e., deformable patch embedding, spatially dynamic self-attention, and multi-scale deformable positional encoding) into a standard ViT-UNet for capturing spatially dynamic information for diverse target objects in the medical image segmentation. Extensive experiments demonstrated the effectiveness of the proposed method for a variety of medical image segmentation tasks. In addition, our AgileFormer significantly outperformed recent 2D and 3D segmentation methods, setting a new state-of-the-art performance. We aspire that the idea of systematically introducing spatially dynamic components to ViT-UNet will guide future designs on how to extract spatially dynamic representations for medical image segmentation with multiple targets, which involve heterogeneous appearances.

References

- [1] Michela Antonelli, Annika Reinke, Spyridon Bakas, Keyvan Farahani, Annette Kopp-Schneider, Bennett A Landman, Geert Litjens, Bjoern Menze, Olaf Ronneberger, Ronald M Summers, et al. The medical segmentation decathlon. *Nature communications*, 13(1):4128, 2022. 6
- [2] Reza Azad, Moein Heidari, Moein Shariatnia, Ehsan Khodapanah Aghdam, Sanaz Karimijafarbigloo, Ehsan Adeli, and Dorit Merhof. Transdeeplab: Convolution-free transformer-based deeplab v3+ for medical image segmentation. In *International Workshop on PRedictive Intelligence In MEDicine*, pages 91–102. Springer, 2022. 6
- [3] Olivier Bernard, Alain Lalande, Clement Zotti, Frederick Cervenansky, Xin Yang, Pheng-Ann Heng, Irem Cetin, Karim Lekadir, Oscar Camara, Miguel Angel Gonzalez Ballester, et al. Deep learning techniques for automatic mri cardiac multi-structures segmentation and diagnosis: is the problem solved? *IEEE transactions on medical imaging*, 37(11):2514–2525, 2018. 6
- [4] Hu Cao, Yueyue Wang, Joy Chen, Dongsheng Jiang, Xiaopeng Zhang, Qi Tian, and Manning Wang. Swin-unet: Unet-like pure transformer for medical image segmentation. In *European conference on computer vision*, pages 205–218. Springer, 2022. 1, 3, 4, 5, 6, 7
- [5] Jieneng Chen, Yongyi Lu, Qihang Yu, Xiangde Luo, Ehsan Adeli, Yan Wang, Le Lu, Alan L Yuille, and Yuyin Zhou. Transunet: Transformers make strong encoders for medical image segmentation. *arXiv preprint arXiv:2102.04306*, 2021. 1, 2, 3, 5, 6, 7, 15
- [6] Xiangxiang Chu, Zhi Tian, Bo Zhang, Xinlong Wang, and Chunhua Shen. Conditional positional encodings for vision transformers. In *The Eleventh International Conference on Learning Representations*, 2022. 5
- [7] Jifeng Dai, Haozhi Qi, Yuwen Xiong, Yi Li, Guodong Zhang, Han Hu, and Yichen Wei. Deformable convolutional networks. In *Proceedings of the IEEE international conference on computer vision*, pages 764–773, 2017. 4
- [8] Alexey Dosovitskiy, Lucas Beyer, Alexander Kolesnikov, Dirk Weissenborn, Xiaohua Zhai, Thomas Unterthiner, Mostafa Dehghani, Matthias Minderer, Georg Heigold, Sylvain Gelly, et al. An image is worth 16x16 words: Transformers for image recognition at scale. In *International Conference on Learning Representations*, 2020. 2, 3
- [9] Ali Hassani, Steven Walton, Jiachen Li, Shen Li, and Humphrey Shi. Neighborhood attention transformer. In *Proceedings of the IEEE/CVF Conference on Computer Vision and Pattern Recognition*, pages 6185–6194, 2023. 4, 5
- [10] Ali Hatamizadeh, Vishwesh Nath, Yucheng Tang, Dong Yang, Holger R Roth, and Daguang Xu. Swin unetr: Swin transformers for semantic segmentation of brain tumors in mri images. In *International MICCAI Brainlesion Workshop*, pages 272–284. Springer, 2021. 2, 3, 6, 7, 15
- [11] Ali Hatamizadeh, Yucheng Tang, Vishwesh Nath, Dong Yang, Andriy Myronenko, Bennett Landman, Holger R Roth, and Daguang Xu. Unetr: Transformers for 3d medical image segmentation. In *Proceedings of the IEEE/CVF winter conference on applications of computer vision*, pages 574–584, 2022. 3, 6, 7, 14, 15
- [12] Moein Heidari, Amirhossein Kazerouni, Milad Soltany, Reza Azad, Ehsan Khodapanah Aghdam, Julien Cohen-Adad, and Dorit Merhof. Hiformer: Hierarchical multi-scale

- representations using transformers for medical image segmentation. In *Proceedings of the IEEE/CVF Winter Conference on Applications of Computer Vision*, pages 6202–6212, 2023. 3, 5, 6
- [13] Huimin Huang, Lanfen Lin, Ruofeng Tong, Hongjie Hu, Qiaowei Zhang, Yutaro Iwamoto, Xianhua Han, Yen-Wei Chen, and Jian Wu. Unet 3+: A full-scale connected unet for medical image segmentation. In *ICASSP 2020-2020 IEEE international conference on acoustics, speech and signal processing (ICASSP)*, pages 1055–1059. IEEE, 2020. 2
- [14] Huaibo Huang, Xiaoqiang Zhou, Jie Cao, Ran He, and Tieniu Tan. Vision transformer with super token sampling. In *Proceedings of the IEEE/CVF Conference on Computer Vision and Pattern Recognition*, pages 22690–22699, 2023. 4
- [15] Jiahao Huang, Xiaodan Xing, Zhifan Gao, and Guang Yang. Swin deformable attention u-net transformer (sdaut) for explainable fast mri. In *International Conference on Medical Image Computing and Computer-Assisted Intervention*, pages 538–548. Springer, 2022. 3, 6, 7, 14
- [16] Xiaohong Huang, Zhifang Deng, Dandan Li, Xueguang Yuan, and Ying Fu. Missformer: An effective transformer for 2d medical image segmentation. *IEEE Transactions on Medical Imaging*, 2022. 3, 6, 7
- [17] Fabian Isensee, Paul F Jaeger, Simon AA Kohl, Jens Petersen, and Klaus H Maier-Hein. nnu-net: a self-configuring method for deep learning-based biomedical image segmentation. *Nature methods*, 18(2):203–211, 2021. 2, 3, 6, 7, 14, 15
- [18] Fabian Isensee, Philipp Kickingereder, Wolfgang Wick, Martin Bendszus, and Klaus H Maier-Hein. Brain tumor segmentation and radiomics survival prediction: Contribution to the brats 2017 challenge. In *Brainlesion: Glioma, Multiple Sclerosis, Stroke and Traumatic Brain Injuries: Third International Workshop, BrainLes 2017, Held in Conjunction with MICCAI 2017, Quebec City, QC, Canada, September 14, 2017, Revised Selected Papers 3*, pages 287–297. Springer, 2018. 2, 5
- [19] Bennett Landman, Zhoubing Xu, J Igelsias, Martin Styner, T Langerak, and Arno Klein. Miccai multi-atlas labeling beyond the cranial vault—workshop and challenge. In *Proc. MICCAI Multi-Atlas Labeling Beyond Cranial Vault—Workshop Challenge*, volume 5, page 12, 2015. 6
- [20] Ho Hin Lee, Shunxing Bao, Yuankai Huo, and Bennett A Landman. 3d ux-net: A large kernel volumetric convnet modernizing hierarchical transformer for medical image segmentation. *arXiv preprint arXiv:2209.15076*, 2022. 2
- [21] Hao Li, Yang Nan, and Guang Yang. Lkai-net: 3d large-kernel attention-based u-net for automatic mri brain tumor segmentation. In *Annual conference on medical image understanding and analysis*, pages 313–327. Springer, 2022. 2
- [22] Ziqiang Li, Hong Pan, Yaping Zhu, and A Kai Qin. Pgd-unet: A position-guided deformable network for simultaneous segmentation of organs and tumors. In *2020 International Joint Conference on Neural Networks (IJCNN)*, pages 1–8. IEEE, 2020. 2
- [23] Ze Liu, Yutong Lin, Yue Cao, Han Hu, Yixuan Wei, Zheng Zhang, Stephen Lin, and Baining Guo. Swin transformer: Hierarchical vision transformer using shifted windows. In *Proceedings of the IEEE/CVF international conference on computer vision*, pages 10012–10022, 2021. 2, 3
- [24] Zhuang Liu, Hanzi Mao, Chao-Yuan Wu, Christoph Feichtenhofer, Trevor Darrell, and Saining Xie. A convnet for the 2020s. In *Proceedings of the IEEE/CVF conference on computer vision and pattern recognition*, pages 11976–11986, 2022. 3
- [25] Ilya Loshchilov and Frank Hutter. Decoupled weight decay regularization. *arXiv preprint arXiv:1711.05101*, 2017. 7
- [26] Ozan Oktay, Jo Schlemper, Loic Le Folgoc, Matthew Lee, Mattias Heinrich, Kazunari Misawa, Kensaku Mori, Steven McDonagh, Nils Y Hammerla, Bernhard Kainz, et al. Attention u-net: Learning where to look for the pancreas. *arXiv preprint arXiv:1804.03999*, 2018. 2, 6, 9
- [27] Md Mostafijur Rahman and Radu Marculescu. Medical image segmentation via cascaded attention decoding. In *Proceedings of the IEEE/CVF Winter Conference on Applications of Computer Vision*, pages 6222–6231, 2023. 3, 6, 7
- [28] Md Mostafijur Rahman and Radu Marculescu. G-cascade: Efficient cascaded graph convolutional decoding for 2d medical image segmentation. In *Proceedings of the IEEE/CVF Winter Conference on Applications of Computer Vision*, pages 7728–7737, 2024. 3, 6
- [29] Md Mostafijur Rahman and Radu Marculescu. Multi-scale hierarchical vision transformer with cascaded attention decoding for medical image segmentation. In *Medical Imaging with Deep Learning*, pages 1526–1544. PMLR, 2024. 2, 3, 5, 6, 7, 11, 12, 14
- [30] Olaf Ronneberger, Philipp Fischer, and Thomas Brox. U-net: Convolutional networks for biomedical image segmentation. In *MICCAI 2015: 18th International Conference, Munich, Germany, October 5-9, 2015, Proceedings, Part III 18*, pages 234–241. Springer, 2015. 2, 6, 9
- [31] Holger R Roth, Hirohisa Oda, Yuichiro Hayashi, Masahiro Oda, Natsuki Shimizu, Michitaka Fujiwara, Kazunari Misawa, and Kensaku Mori. Hierarchical 3d fully convolutional networks for multi-organ segmentation. *arXiv preprint arXiv:1704.06382*, 2017. 3
- [32] Saikat Roy, Gregor Koehler, Constantin Ulrich, Michael Baumgartner, Jens Petersen, Fabian Isensee, Paul F Jaeger, and Klaus H Maier-Hein. Mednext: transformer-driven scaling of convnets for medical image segmentation. In *International Conference on Medical Image Computing and Computer-Assisted Intervention*, pages 405–415. Springer, 2023. 3, 7, 15
- [33] Abdelrahman M Shaker, Muhammad Maaz, Hanoona Rasheed, Salman Khan, Ming-Hsuan Yang, and Fahad Shahbaz Khan. Unetr++: delving into efficient and accurate 3d medical image segmentation. *IEEE Transactions on Medical Imaging*, 2024. 7, 15
- [34] Peter Shaw, Jakob Uszkoreit, and Ashish Vaswani. Self-attention with relative position representations. In *Proceedings of NAACL-HLT*, pages 464–468, 2018. 5
- [35] Zhengzhong Tu, Hossein Talebi, Han Zhang, Feng Yang, Peyman Milanfar, Alan Bovik, and Yinxiao Li. Maxvit: Multi-axis vision transformer. In *European conference on computer vision*, pages 459–479. Springer, 2022. 11

- [36] Haonan Wang, Peng Cao, Jiaqi Wang, and Osmar R Zaiane. Utransnet: rethinking the skip connections in u-net from a channel-wise perspective with transformer. In *Proceedings of the AAAI conference on artificial intelligence*, volume 36, pages 2441–2449, 2022. 2, 4
- [37] Hongyi Wang, Shiao Xie, Lanfen Lin, Yutaro Iwamoto, Xian-Hua Han, Yen-Wei Chen, and Ruofeng Tong. Mixed transformer u-net for medical image segmentation. In *ICASSP*, pages 2390–2394. IEEE, 2022. 6, 7
- [38] Wenxuan Wang, Chen Chen, Meng Ding, Hong Yu, Sen Zha, and Jiangyun Li. Transbts: Multimodal brain tumor segmentation using transformer. In *MICCAI 2021: 24th International Conference, Strasbourg, France, September 27–October 1, 2021, Proceedings, Part I 24*, pages 109–119. Springer, 2021. 3, 5, 7
- [39] Zhuofan Xia, Xuran Pan, Shiji Song, Li Erran Li, and Gao Huang. Vision transformer with deformable attention. In *Proceedings of the IEEE/CVF conference on computer vision and pattern recognition*, pages 4794–4803, 2022. 3, 4, 11, 12
- [40] Zhuofan Xia, Xuran Pan, Shiji Song, Li Erran Li, and Gao Huang. Dat++: Spatially dynamic vision transformer with deformable attention. *arXiv preprint arXiv:2309.01430*, 2023. 2, 3
- [41] Yutong Xie, Jianpeng Zhang, Chunhua Shen, and Yong Xia. Cotr: Efficiently bridging cnn and transformer for 3d medical image segmentation. In *MICCAI 2021: 24th International Conference, Strasbourg, France, September 27–October 1, 2021, Proceedings, Part III 24*, pages 171–180. Springer, 2021. 2, 3, 6, 7, 11, 14, 15
- [42] Xiangyi Yan, Hao Tang, Shanlin Sun, Haoyu Ma, Deyang Kong, and Xiaohui Xie. After-unet: Axial fusion transformer unet for medical image segmentation. In *Proceedings of the IEEE/CVF winter conference on applications of computer vision*, pages 3971–3981, 2022. 6
- [43] Jin Yang, Peijie Qiu, Yichi Zhang, Daniel S Marcus, and Aristeidis Sotiras. D-net: Dynamic large kernel with dynamic feature fusion for volumetric medical image segmentation. *arXiv preprint arXiv:2403.10674*, 2024. 2
- [44] Chenyu You, Ruihan Zhao, Fenglin Liu, Siyuan Dong, Sandeep Chinchali, Ufuk Topcu, Lawrence Staib, and James Duncan. Class-aware adversarial transformers for medical image segmentation. *Advances in Neural Information Processing Systems*, 35:29582–29596, 2022. 6
- [45] Zhengxin Zhang, Qingjie Liu, and Yunhong Wang. Road extraction by deep residual u-net. *IEEE Geoscience and Remote Sensing Letters*, 15(5):749–753, 2018. 2
- [46] Hengshuang Zhao, Jianping Shi, Xiaojuan Qi, Xiaogang Wang, and Jiaya Jia. Pyramid scene parsing network. In *Proceedings of the IEEE conference on computer vision and pattern recognition*, pages 2881–2890, 2017. 3
- [47] Hong-Yu Zhou, Jiansen Guo, Yinghao Zhang, Xiaoguang Han, Lequan Yu, Liansheng Wang, and Yizhou Yu. nn-former: Volumetric medical image segmentation via a 3d transformer. *IEEE Transactions on Image Processing*, 2023. 1, 2, 3, 4, 5, 6, 7, 14, 15
- [48] Zongwei Zhou, Md Mahfuzur Rahman Siddiquee, Nima Tajbakhsh, and Jianming Liang. Unet++: Redesigning skip

connections to exploit multiscale features in image segmentation. *IEEE transactions on medical imaging*, 39(6):1856–1867, 2019. 2

- [49] Xizhou Zhu, Weijie Su, Lewei Lu, Bin Li, Xiaogang Wang, and Jifeng Dai. Deformable detr: Deformable transformers for end-to-end object detection. In *International Conference on Learning Representations*, 2020. 2, 11

Appendix

A. Comparison to CoTr [41] and MERIT [29]

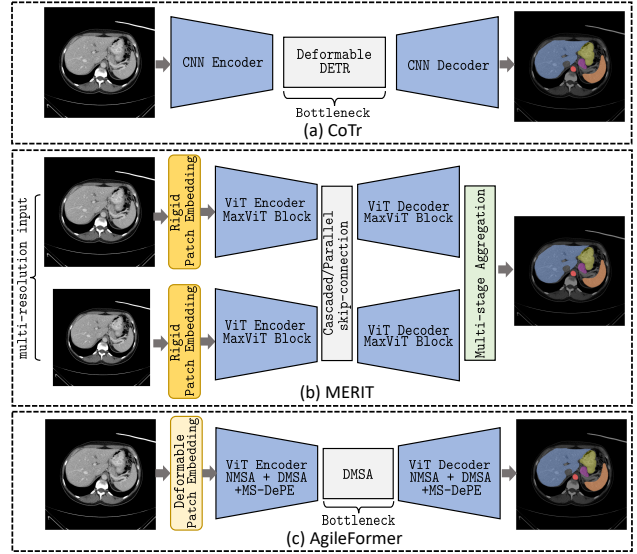


Figure S1. (a) CoTr is a hybrid model where Deformable DETR [49] is only applied to the bottleneck. (b) MERIT captures dynamic feature representations using a multi-resolution and multi-stage approach, with the MaxViT [35] as the building block. (c) AgileFormer alternates NMSA and DMSA as the building block, adding novel deformable patch embedding and multi-scale deformable positional encoding.

A.1. Comparison to CoTr [41]

Similar to its ancestor model [49], CoTr is a hybrid model where the main backbone (encoder/decoder) is still a CNN. Multi-scale deformable attention outlined in [49] serves as a bottleneck (see Fig. S1 (a)). As a result, it can only introduce limited deformability to capture spatially dynamic feature representations, as the main feature extractor does not have spatially dynamic components. In addition, CoTr does not take full advantage of ViT to capture long-range dependencies as its main backbone is still a CNN. We hypothesized that these factors may limit its performance and scalability. Instead, the proposed method uses a pure ViT as the main backbone (encoder/decoder), where neighborhood attention and deformable attention [39] serve as the main building blocks (see Fig. S1 (c)). This better preserves

Table S1. Optimal training hyperparameter and model configurations for different experimental settings.

Models		training hyperparameters				model configuratoins		
		learning rate	epochs	batch size	weight balance parameter λ	first deformable patch embedding strides	downsampling patch embedding strides	input size
2D	AgileFormer-B [Synapse multi-organ]	2e-4	400	24	0.6	[2, 2], [2, 2]	[2, 2], [2, 2], [2, 2]	224×224
	AgileFormer-B [ACDC cardiac]	4e-4	400	24	0.6	[2, 2], [2, 2]	[2, 2], [2, 2], [2, 2]	224×224
3D	AgileFormer-T [Synapse multi-organ]	2e-4	1000	4	0.5	[1, 2, 2], [2, 2, 2]	[2, 2, 2], [2, 2, 2], [2, 2, 2]	$64 \times 128 \times 128$
	AgileFormer-T [ACDC cardiac]	3e-4	1000	4	0.5	[1, 2, 2], [2, 2, 2]	[1, 2, 2], [1, 2, 2], [2, 2, 2]	$14 \times 160 \times 160$
	AgileFormer-T [Decathlon brain tumor]	5e-4	200	4	0.5	[2, 2, 2], [2, 2, 2]	[2, 2, 2], [2, 2, 2], [2, 2, 2]	$96 \times 96 \times 96$

Table S2. Ablation studies on model design variants in Synapse multi-organ segmentation task, starting from a SwinUNet baseline. This is also the roadmap going from SwinUNet to the proposed AgileFormer.

	Avg DSC \uparrow	Aorta	Gallbladder	Kidney(L)	Kidney(R)	Liver	Pancreas	Spleen	Stomach	Parms (M) / FLOPs (G)
Baseline (WMSA + RPE)	79.13	85.47	66.53	83.28	79.61	94.29	56.58	90.66	76.60	27.17 / 6.13
Convolutional Downsampling	79.40	85.74	70.56	82.33	80.69	93.50	58.89	91.46	72.05	29.10 / 6.34
Deformable Patch Embedding	80.91	87.38	71.25	85.17	83.08	94.11	58.71	88.92	78.67	29.14 / 6.54
NMSA + WMSA (w/o PE)	81.27	87.22	68.79	84.73	79.49	95.31	63.13	90.62	80.86	26.74 / 6.31
WMSA + DMSA (w/o PE)	81.47	86.12	67.37	84.18	80.13	95.61	64.86	90.97	82.55	26.77 / 5.98
NMSA + DMSA (w/o PE)	82.06	87.54	70.95	81.90	79.29	95.36	68.03	90.72	82.72	26.82 / 5.99
+ APE	81.96	88.35	70.72	81.82	78.84	95.09	67.80	90.27	82.45	28.90 / 5.99
APE \rightarrow deformable RPE [39]	82.42	87.17	73.32	86.08	82.54	95.08	65.65	88.64	80.92	26.99 / 6.00
deformable RPE \rightarrow CPE	81.91	88.13	72.28	79.81	77.75	95.06	65.24	91.90	85.14	26.87 / 6.01
CPE \rightarrow MS-DePE	82.74	88.08	75.16	82.41	81.36	95.09	67.23	90.94	81.61	27.47 / 7.08
+ Deep Supervision	83.59	88.81	74.43	84.61	82.78	95.48	69.45	90.14	83.05	28.85 / 7.36

the advantage of ViT while having the additional advantage of capturing spatially localized and dynamic features. This accounts for the superior performance of AgileFormer compared to CoTr. In particular, AgileFormer outperforms CoTr by 5.03, 1.24, and 1.6 in DSC (%) for multi-organ, cardiac, and brain tumor segmentations, respectively.

A.2. Comparison to MERIT [29]

MERIT mainly takes advantage of multi-resolution inputs to capture representation at multiple scales (see Fig. S1 (b)). This is achieved by combining the features extracted from inputs of different sizes. As a result, MERIT mainly models targets with varying sizes but may fail to capture objects with varying shapes. Instead, our AgileFormer handles both varying sizes as well as varying shapes by deformable patch embedding and spatially dynamic attention (see Fig. S1 (c)). In addition, we proposed a multi-scale deformable positional encoding to further capture multi-scale information. Consequently, AgileFormer outperforms MERIT by 0.84 and 0.23 in DSC (%) for multi-organ and cardiac segmentation, respectively.

More comparisons: We would like to point out that the official implementation² of MERIT used test set to select the best model on Synapse. In contrast, we did not use the test set for model selection and only evaluated the model checkpoint at the last training epoch. As stated in Table 1, if using the test set to select the best model, Agileformer can achieve

²<https://github.com/SLDGroup/MERIT>

an average DSC (%) of 86.11 (vs. 84.90 MERIT). To be more rigorous, if evaluated on the last training checkpoint, MERIT only achieved a DSC (%) of 82.89 (vs. 85.74 AgileFormer) on Synapse. Therefore, the improvement over MERIT is not marginal but statistically significant.

B. Additional Implementation Details

The model configurations and optimal training hyperparameter settings for 2D and 3D experiments are shown in Table S1. We used different downsampling strides for patch embeddings to accommodate different input sizes. The weight parameters λ balance the DSC loss (\mathcal{L}_{DSC}) and cross-entropy loss ($\mathcal{L}_{\text{cross-entropy}}$) as follows:

$$\mathcal{L} = \lambda \mathcal{L}_{\text{DSC}} + (1 - \lambda) \mathcal{L}_{\text{cross-entropy}}. \quad (4)$$

C. Ablation studies

Here, we provide detailed results for ablation studies in Table S2, including the change of segmentation accuracy, parameters, and floating points (FLOPs).

D. Additional Qualitative Results

Additional qualitative results on Synapse produced by 3D models are shown in Fig. S2, where AgileFormer showcased accurate segmentation compared to other state-of-the-art methods. Some failure cases on Synapse are shown in Fig. S3, where even methods that can extract spatially dynamic features (including AgileFormer) cannot accurately

segment highly irregular organs such as Gallbladder and Pancreas. Similarly, Fig. S4 shows failure cases on brain tumor segmentation tasks, where tissue classes with highly irregular appearance cannot be accurately segmented by most methods, including AgileFormer.

E. Statistical Test

On Synapse, we performed the Wilcoxon signed rank test to the second-best model (i.e., 2D MERIT and 3D nnUNet), where the populations are the DSC values for 8 different organs. However, on ACDC and Decathlon datasets, we performed the paired t-test to the second-best model, as there are only three foreground labels. In these two cases, the populations were the DSC values for all subjects across the dataset.

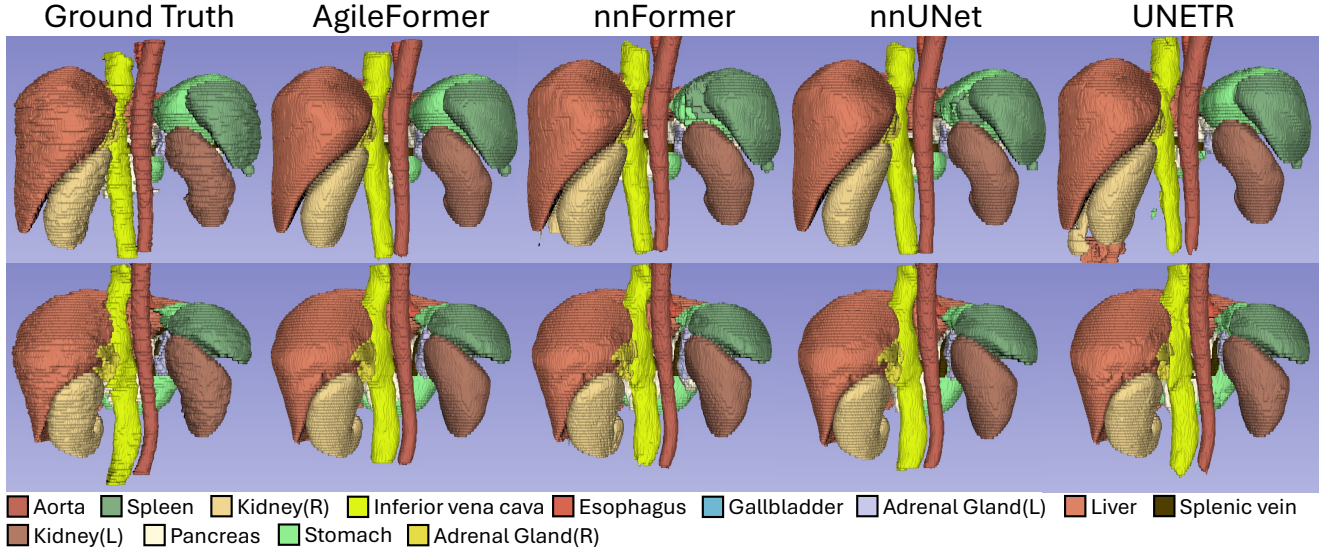


Figure S2. Qualitative comparison between the proposed AgileFormer, nnFormer [47], nnUNet [17], and UNETR [11] on the Synapse multi-organ segmentation task.

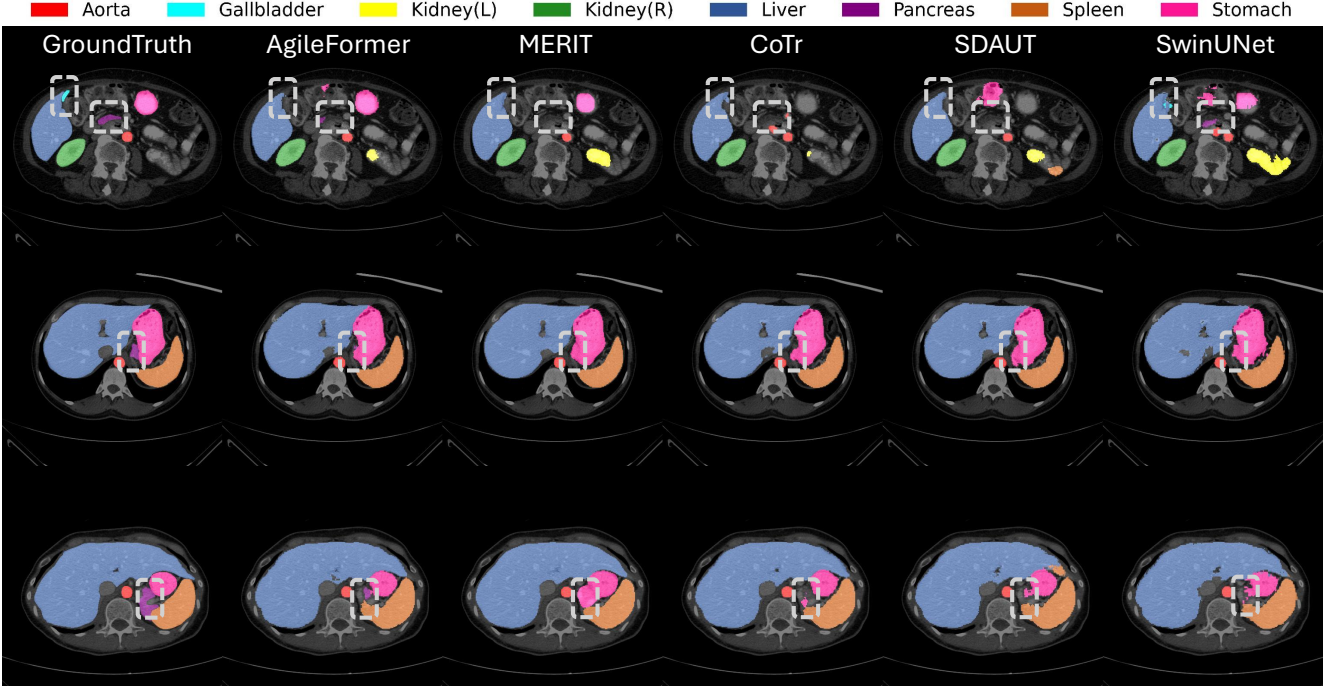


Figure S3. Failure cases where accurately segmenting irregular organs like the gallbladder and pancreas (highlighted by gray boxes) is challenging for most methods with spatially dynamic components [15, 29, 41], including AgileFormer.

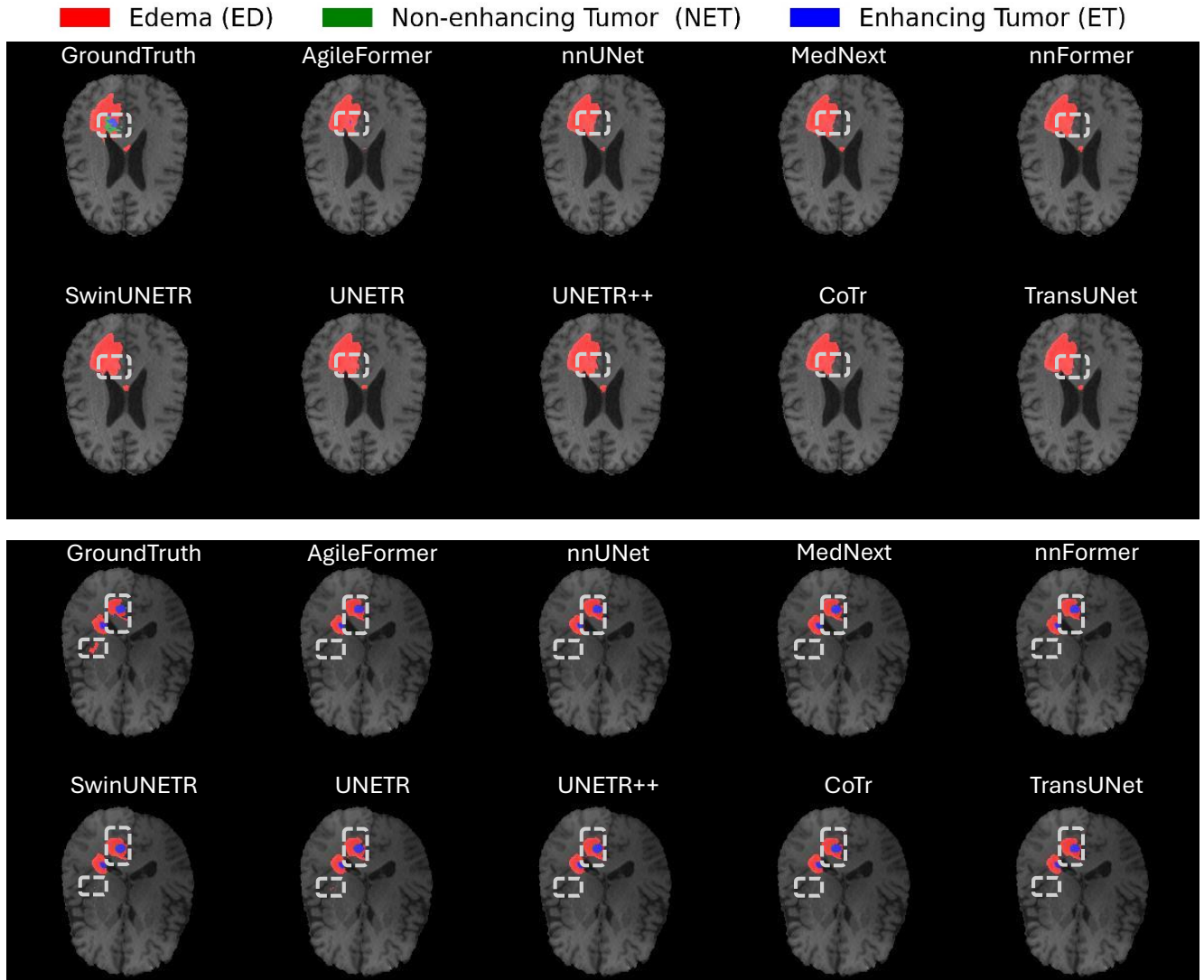


Figure S4. Failure cases where accurately segmenting irregular tumor tissues (highlighted by gray boxes) is challenging for most methods [5, 10, 11, 17, 32, 33, 41, 47], including AgileFormer.